

Freehand three-dimensional ultrasound to assess semitendinosus muscle morphology

Helga Haberfehlner,^{1,2} Huub Maas,¹ Jaap Harlaar,² Jules G. Becher,² Annemieke I. Buizer² and Richard T. Jaspers¹

¹Laboratory for Myology, Department of Human Movement Sciences, Faculty of Behavioural and Movement Sciences, Vrije Universiteit Amsterdam, MOVE Research Institute Amsterdam, The Netherlands

²Department of Rehabilitation Medicine, VU University Medical Center, MOVE Research Institute Amsterdam, The Netherlands

Abstract

In several neurological disorders and muscle injuries, morphological changes of the m. semitendinosus (ST) are presumed to contribute to movement limitations around the knee. Freehand three-dimensional (3D) ultrasound (US), using position tracking of two-dimensional US images to reconstruct a 3D voxel array, can be used to assess muscle morphology *in vivo*. The aims of this study were: (i) to introduce a newly developed 3D US protocol for ST; and (ii) provide a first comparison of morphological characteristics determined by 3D US with those measured on dissected cadaveric muscles. Morphological characteristics of ST (e.g. muscle belly length, tendon length, fascicle length and whole muscle volume, and volumes of both compartments) were assessed in six cadavers using a 3D US protocol. Subsequently, ST muscles were removed from the body to measure the same morphological characteristics. Mean differences between morphological characteristics measured by 3D US and after dissection were smaller than 10%. Intra-class correlation coefficients (ICCs) were higher than 0.75 for all variables except for the lengths of proximal fascicles (ICC = 0.58). Measurement of the volume of proximal compartment by 3D US was not feasible, due to low US image quality proximally. We conclude that the presented 3D US protocol allows for reasonably accurate measurements of key morphological characteristics of ST muscle.

Key words: three-dimensional ultrasonography; geometry; hamstrings; muscle architecture.

Introduction

The semitendinosus muscle (ST) is one of the medial hamstring muscles, spanning the hip as well as the knee joint. Morphological changes of ST are observed in several central neurological disorders (e.g. cerebral palsy, stroke, multiple sclerosis, traumatic brain injury; Keenan et al. 1988; Martin et al. 2006; Gage et al. 2009), following sport injuries (Silder et al. 2008) as well as after surgery (e.g. anterior cruciate ligament reconstruction with the ST tendon; Nishino et al. 2006), and are presumed to contribute to movement limitations around the knee. As the morphology of a muscle is a major determinant of its mechanical properties (Gans & Bock, 1965; Woittiez et al. 1983; Brand et al. 1986; Gans &

Gaunt, 1991; Huijing, 1996; Winters et al. 2011), knowledge of ST morphology may improve our understanding of ST function. Freehand three-dimensional ultrasound (3D US) has been shown to allow for accurate and standardized assessment of: (i) length of morphological variables (Fry et al. 2004; Barber et al. 2009; Weide et al. 2015); and (ii) muscle volume (Weller et al. 2007; Barber et al. 2009; MacGillivray et al. 2009). Currently for ST no specific 3D US protocol is available.

The ST is divided by a tendinous inscription (also referred to as raphe) into a proximal and a distal compartment (Markee et al. 1955; Lee et al. 1988; Woodley & Mercer, 2005; Kellis et al. 2012; van der Made et al. 2013). Fascicles in both ST compartments are arranged in series and exert force at a small angle with the aponeuroses (Kellis et al. 2009; Ward et al. 2009). To assess morphological characteristics of ST by 3D US, detailed knowledge about ST morphology needs to be taken into account.

The aims of this study were to: (i) introduce a newly developed 3D US protocol for ST; and (ii) provide a first comparison of morphological characteristics determined by 3D US data with those measured on dissected cadaveric muscles.

Correspondence

Richard T. Jaspers, Laboratory for Myology, Department of Human Movement Sciences, Faculty of Behavioural and Movement Sciences, Vrije Universiteit Amsterdam, MOVE Research Institute Amsterdam, Van der Boerhorststraat 9, 1081 BT Amsterdam, The Netherlands.
E: r.t.jaspers@vu.nl

Accepted for publication 29 April 2016
Article published online 6 June 2016

Materials and methods

Data were collected using six human cadavers [one female, five males, age at death 81.5 ± 9.5 years, mean \pm standard deviation (SD)]. The cadavers were obtained from the donation program of the Department of Anatomy and Neurosciences of the VU University Medical Center (VUmc), Amsterdam, The Netherlands. The bodies were formalin-preserved with hip and knee joints in extended position. Extension in the joint was not forced. Therefore, knee and hip joints were in a slightly flexed position (i.e. hip: $8.8 \pm 1.8^\circ$; knee: $4.2 \pm 5.8^\circ$). To measure knee and hip angles, an extendable goniometer with two moveable arms was used (Model 01135, Lafayette Instrument, USA). Upper leg length, defined as the linear distance between the trochanter major and the most prominent part of the lateral epicondyle of the femur, was 39.0 ± 3.2 cm and measured by a 1 m ruler with mm increments.

US imaging and volume reconstruction

Prior to anatomical dissection, US imaging of ST muscle was performed freehand using a B-mode US apparatus with a 5 cm linear probe (Technos MPX, ESAOTE S.p.A., Italy). The scanning area was covered with a thick layer (≈ 5 mm) of US gel (Transsound, EF Medica Sri, Italy) to improve image quality. A 30–40 s sequence of transverse US images (i.e. axial plane of the ST muscle) was collected starting distally at the ST tendon (i.e. at the point that the tendon could be sufficiently visualized in the popliteal fossa) ending at the origin on the ischial tuberosity. None of the ST muscles of the cadavers was wider than 5 cm, therefore it was possible to measure all muscles by a single sweep using a 5-cm linear probe. The US images were sampled at a rate of 25 Hz using a video card and capturing software (miroVIDEO DC30; Pinnacle Systems). The position of each US image in 3D space was recorded by tracking the US probe (based on three-markers that were rigidly attached to it) using an Optotrak motion capture system (type 3020; Northern Digital, Waterloo, Canada). Positions of selected bony anatomical landmarks (i.e. most prominent part of the ischial tuberosity, lateral and medial epicondyle) were recorded prior to scanning using an optically six-marker rigid body optotrak-pointer (also referred to as optotrak-probe; Optotrak, Northern Digital, Waterloo, Canada). All three bony landmarks were identified by palpation and confirmed by US. If this was not possible for the ischial tuberosity, the location was confirmed by pricking a needle. Prior to 3D US imaging of the cadavers, the transformation matrix from the probe frame to the US images was determined within the US images by identifying a cross-point of two intersecting wires at a known position in a water cube. The cross of the wire was scanned from different positions and with different tilt angles of the US probe, while the cross-wire was kept visible within the recorded US image sequence (Prager et al. 1998). The propagation speed of sound in muscle tissue at body temperature (i.e. 1570 m s^{-1}) is different from that in water due to density differences, and is temperature dependent. The temperature of the water was measured using a digital thermometer (GTH 175/PT, Greisinger, Germany), and the speed of sound in water was set according to the corresponding temperature. The cadaveric bodies were allowed to warm up to the temperature in the dissection room (about 18°C) for 4–6 h and propagation speed was set to 1532 m s^{-1} , according to a temperature of 18°C (Straube & Arthur, 1994), in the reconstruction process. No corrections were made for possible differences in propagation speed due to formalin preservation of the cadavers, because effects have been shown to be very low (Bamber et al. 1979; Baldwin et al. 2006).

A custom-made program in Matlab (version R2014A, the Mathworks) was used to fill a 3D voxel array with pixels from the transverse US images (Bénard et al. 2011) for later analysis (see below). Missing information was interpolated using nearest-neighborhood interpolation. The size of a voxel was 0.2×0.2 mm for the transverse direction and approximately 0.5 mm longitudinally (dependent on the sliding velocity of the probe and, hence, the number of images collected).

Anatomical dissection to measure morphological characteristics of cadaveric ST

After US imaging skin, subcutaneous tissues, gluteus muscle and fasciae of ST, semimembranosus and biceps femoris muscles were removed (Fig. 1A). The location, where the distal ST tendon passed the knee axis of rotation (i.e. defined as the line between medial and lateral epicondyles), was marked with a suture on the ST tendon. Then ST was carefully dissected from its origin at the ischial tuberosity and at its insertion at the tibia as close as possible to the bone.

The following morphological characteristics of ST muscle-tendon unit (MTU) were measured: muscle belly length (ℓ_m), the distance from ischial tuberosity to distal end of muscle belly; distal tendon length ($\ell_{t_{\text{dist}}}$), the distance from the distal end of the most distal fascicle to the insertion at the pes anserinus; distal tendon length proximal to the knee axis ($\ell_{t_{\text{dist-p}}}$), i.e. the length of the distal tendon from the distal end of the most distal fascicles to the knee axis; and the length of the portion of the tendinous inscription that was visible externally of the muscle belly ($\ell_{t_{\text{external}}}$). In a pilot study, ℓ_m was measured in five cadavers before and after removal of ST from the skeleton. Measurements confirmed that ℓ_m after dissection did not differ from that *in situ* (difference = 0.02 ± 0.53 cm; $P = 0.944$).

For further measurements, the muscle belly was longitudinally cut in two halves. The blade was orientated perpendicularly to the apical surface of the oval-shaped distal aponeurosis. The muscle was cut towards the proximal end of the tendinous inscription (Fig. 1B). The longitudinal sections were positioned on a table, aligned with the distal and proximal ends, and left in the shape defined by formalin fixation within the body (Fig. 1C). Within the plane of the longitudinal section of ST, the following anatomical length variables were measured using a ruler with mm increments: distal aponeurosis length ($\ell_{a_{\text{dist}}}$); proximal aponeurosis length ($\ell_{a_{\text{prox}}}$); length of tendinous inscription (ℓ_{ti}); within the distal muscle compartment the lengths of the most distal ($\ell_{\text{fasc}_{\text{dist-d}}}$), intermediate ($\ell_{\text{fasc}_{\text{dist-m}}}$) and most proximal fascicles ($\ell_{\text{fasc}_{\text{dist-p}}}$); and within the proximal compartment lengths of the most distal ($\ell_{\text{fasc}_{\text{prox-d}}}$), intermediate ($\ell_{\text{fasc}_{\text{prox-m}}}$) and most proximal fascicles ($\ell_{\text{fasc}_{\text{prox-p}}}$) (Fig. 1D). In addition, by using a protractor, the angle of the most distal fascicles of the distal compartment with the muscle line of pull (α_{dist}), the angle of the distal aponeurosis with the muscle line of pull (β_{dist}), the angle of the most proximal fascicles of the proximal compartment with the muscle line of pull (α_{prox}), and the angle of the proximal aponeurosis with the muscle line of pull (β_{prox}) were determined. The muscle line of pull was defined as the line between the proximal end of the most proximal fascicles and the distal end of the most distal fascicle (Fig. 1D). Angle gamma (γ) was calculated by summing α and β (γ_{dist} , γ_{prox}). ℓ_m and $\ell_{t_{\text{dist-p}}}$ were summed to assess MTU length up to the estimated knee axis (ℓ_{mtu}). After measuring the morphological characteristics within the mid-longitudinal plane, the muscle was cut perpendicularly to its length at the middle of the projection of the distal and proximal ends of the tendinous inscription. A photograph of the anatomical

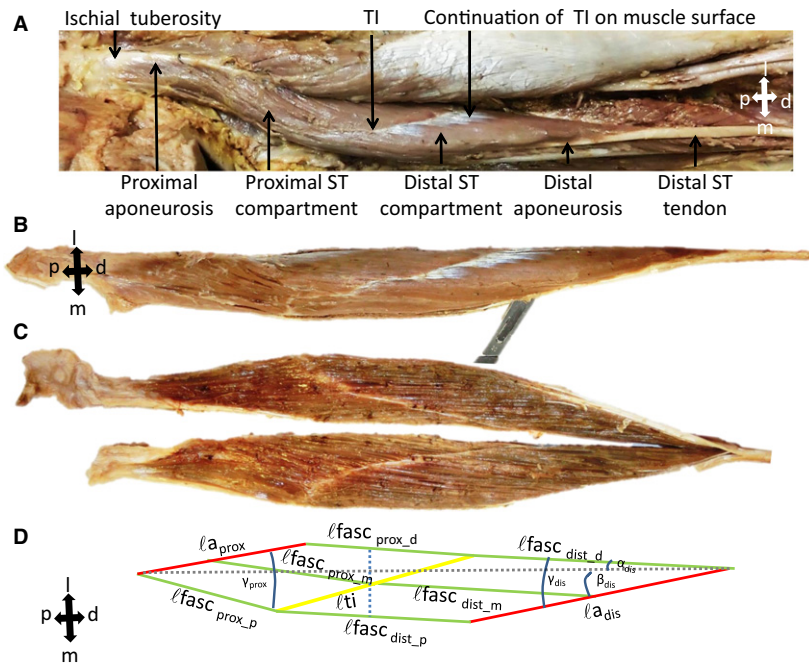


Fig. 1 Typical example of semitendinosus muscle (ST) *in situ*, of a mid-longitudinal transection of ST and illustration of morphological characteristics. (A) The ST was made visible by removing the skin, subcutaneous tissues, gluteus muscle and the fasciae of ST. Posterior view, proximal of knee axis. (B) Photographic image demonstrating the transection. Starting from the distal end of the most distal fascicle, the blade was perpendicularly orientated on the apex of the oval-shaped distal aponeurosis. The muscle was cut in the direction of the proximal end of the tendinous inscription. (C) Photographic image of the longitudinal section of ST. (D) Two-dimensional planimetric model of the morphological variables measured in the mid-longitudinal plane: distal aponeurosis (ℓa_{dist}), proximal aponeurosis (ℓa_{prox}), most distal fascicle of distal compartment ($\ell fasc_{dist_d}$), most proximal fascicles of distal compartment ($\ell fasc_{dist_p}$), most distal fascicle of proximal compartment ($\ell fasc_{prox_d}$), most proximal fascicles of proximal compartment ($\ell fasc_{prox_p}$), intermediate fascicles ($\ell fasc_{dist_m}$, $\ell fasc_{prox_m}$) and tendinous inscription (ℓti). The gray dotted line indicates the location for the transversal section of ST for assessment of anatomical cross-sectional area (ACSA). The blue dotted line indicates the location for the transversal section of ST for assessment of anatomical cross-sectional area (ACSA). d, distal; l, lateral; m, medial; p, proximal; TI, tendinous inscription.

cross-sectional area (ACSA) was taken while a millimeter scale was positioned in the image plane. The ACSA was measured from the image using the open source imaging software Fiji (<http://fiji.sc>; Schindelin et al. 2012; Schneider et al. 2012). Subsequently, the general fascia as well as the distal tendon were removed, leaving solely the muscle belly including the distal and proximal aponeuroses. The proximal and distal compartments of ST were separated by carefully cutting the myotendinous connections of the fascicles from the distal side of the tendinous inscription. The volumes of the distal (Vol_{dist}) and proximal compartments (Vol_{prox}) were measured by submerging them in distilled water ($\approx 20^\circ\text{C}$) within a calibrated measuring cylinder. Vol_{dist} and Vol_{prox} were summed up to obtain the total muscle belly volume of ST (Vol). The lengths of the most distal, intermediate and most proximal fascicles of distal and proximal compartment were summed. The mean of these summed fascicles at each location was calculated and represented the mean fascicle length of the whole muscle ($\ell fasc_{average}$).

From each compartment two fascicle segments of at least 3 cm were carefully dissected from a medial and a lateral location, and stored in a formalin- and ethanol-based solution for later assessment of sarcomere length. From each of these stored fascicles, small fiber bundles were dissected and placed on a microscopic slide. Every 3 mm, photographs were taken using a digital camera (Mikro-Cam 5 MP, Bresser, Rhede, Germany) mounted on a microscope (Ortholux II, Leitz, Wetzlar, Germany). The method used to assess

sarcomere lengths has recently been described (Tijss et al. 2015). The distribution of gray-scale values for a single fiber on each photograph was determined using the plot profile plugin in Fiji. The gray-scale signal was filtered (Butterworth, 5th order) to exclude sarcomere lengths above $4\ \mu\text{m}$ (cut-off frequency: 0.25 sarcomeres per μm) and below $1.5\ \mu\text{m}$ (cut-off frequency: 0.67 sarcomeres per μm). A discrete Fourier transformation was performed in Matlab to determine the number of sarcomeres in series. Subsequently, fiber mean sarcomere lengths were calculated by dividing total fiber length by the number of sarcomeres. If the count of number of sarcomeres in series was not possible automatically due to noise in the sinusoidal wave, measurement of sarcomere lengths was performed using FFT plugin in Fiji. Fiber mean sarcomere lengths were first averaged across fibers from each location within the compartment, then across compartment locations and, subsequently, across both compartments ($\ell sarc$). Fascicle length at estimated optimum sarcomere length ($\ell fasc_{average_optimum}$) was calculated by the following equation.

$$\ell fasc_{average_optimum} = \ell fasc_{average} * (2.7\ \mu\text{m} / \ell sarc) \quad (1)$$

For humans a sarcomere length of $2.7\ \mu\text{m}$ is in between the range that has been described for optimum sarcomere length, $2.67\text{--}2.81\ \mu\text{m}$ (Walker & Schrodt, 1974; Rassier et al. 1999) and $2.60\text{--}2.80\ \mu\text{m}$ (Lieber et al. 1994). The physiological cross-sectional area (PCSA) of

ST, defined as the cross-sectional area of all muscle fibers arranged in parallel, was calculated by dividing Vol by $\ell_{fasc_{average}}$ (PCSA) and by $\ell_{fasc_{average_{optimum}}}$ ($PCSA_{optimum}$), respectively (Alexander & Vernon, 1975). PCSA and $PCSA_{optimum}$ were calculated for both compartments as well as for the whole muscle.

Image analysis 3D US

A 3D US protocol was developed to measure the following subset of morphological characteristics taking into account the two compartments of the ST: ℓ_m , $\ell_{t_{dist_{pr}}}$, $\ell_{a_{dist}}$, $\ell_{fasc_{dist_{dr}}}$, $\ell_{fasc_{dist_{pr}}}$, $\ell_{fasc_{prox_{pr}}}$, Vol_{dist} , Vol_{prox} and ACSA.

Muscle structures (i.e. tendon, distal aponeurosis, tendinous inscription) were identified by visual inspection in three dimensions within the voxel array using open source software Chimera 1.9 (<http://www.cgl.ucsf.edu/chimera>; Pettersen et al. 2004; Fig. 2). Segmentation of ST for assessment of muscle volume was performed using the Segmentation Editor Plugin (http://fiji.sc/Segmentation_Editor) in Fiji. The outline of ST was encircled in transverse images every 5 mm, interpolating the gaps between the segmented images (Weller et al. 2007). Muscle volume was measured using the volume measurement tool in Chimera 1.9. It was planned to segment distal and proximal compartments of ST and assess Vol_{dist} and Vol_{prox} (Fig. 2). However, for all cadavers full segmentation of the Vol_{prox} was not feasible due to insufficient image quality of the most proximal part within the voxel array.

In order to measure the above-specified variables, x , y , z coordinates of the following points were determined within the voxel array in combination with positions of the bony landmarks obtained from the optotrak registration (Fig. 3): ischial tuberosity; most proximal and distal ends of the tendinous inscription; proximal end of the distal aponeurosis; the distal end of the most distal fascicle; and the most distal point of the distal tendon (proximal of

the knee axis). In addition, direction vectors were defined to describe a line between the distal end of the most distal fascicle (indicated as point 7 in Fig. 3) and the most distal visible point of the distal tendon (indicated as point 8 in Fig. 3; i.e. 'line of tendon'), and a line between the medial and lateral epicondyles (i.e. 'line of estimated knee axis'; Fig. 3). The point along the 'line of tendon' from which the distance to the 'line of estimated knee axis' was smallest was taken as an estimate of the crossing of the distal tendon with the knee axis (indicated as point 9 in Fig. 3). Distances between x , y , z coordinates of the above-mentioned points were used to define ℓ_m , $\ell_{t_{dist_{pr}}}$, $\ell_{a_{dist}}$, $\ell_{fasc_{dist_{dr}}}$, $\ell_{fasc_{dist_{pr}}}$, $\ell_{fasc_{prox_{pr}}}$ (Fig. 3). Determination of the ischial tuberosity within the voxel array was not always possible. If the ischial tuberosity was not visible, the position obtained from the optotrak registration was used for further calculations. The ACSA was measured at the middle of the tendinous inscription, perpendicular to the muscle line of pull. $PCSA_{dist}$ was calculated by dividing Vol_{dist} by the average of both measured distal fascicles (i.e. $\ell_{fasc_{dist_{dr}}}$, $\ell_{fasc_{dist_{pr}}}$).

Assessment of the x , y , z coordinates of points at ST within the voxel array (i.e. points 4–8 in Fig. 3) was performed five times by the same observer. Segmentations of the volumes and measurement of ACSA were repeated three times by the same observer. After five repetitions for assessment of x , y , z coordinates of points and three repetitions of analyzing volume of distal compartment and ACSA, the increase of intra-class correlation coefficients (ICC) and the decrease of standard error of measurement (SEM) were minimal. Therefore, these numbers of repetitions were deemed sufficient. ICCs based on five and three repetitions, respectively, were higher than 0.90, SEMs were between 0.5 and 4 mm for the point assessment, 1.5 cm^3 for the distal volume and 0.2 cm^2 for the ACSA. The means of x , y , z coordinates of five observations for the point assessment and of three repetitions of segmentations of the distal volume and measurement of ACSA were used for further calculations.

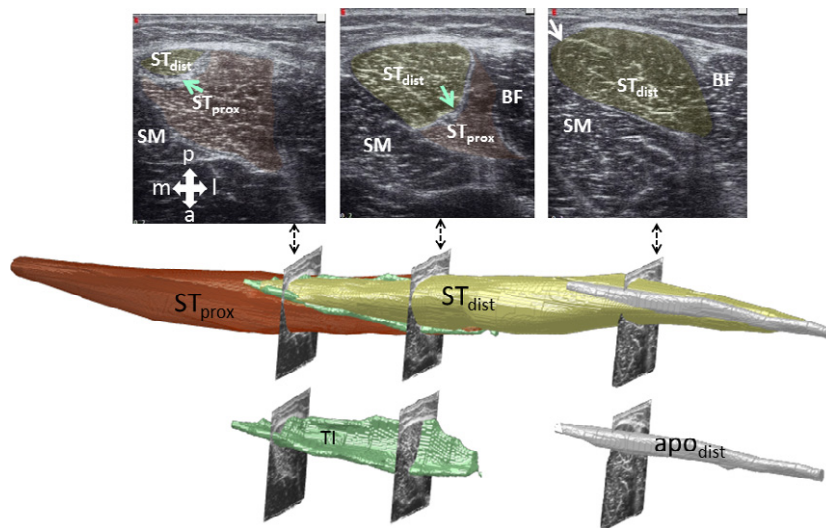


Fig. 2 Typical example of segmented semitendinosus muscle (ST) based on transversal images. ST segmented into the proximal (ST_{prox}) (red) and distal compartment (ST_{dist}) (yellow), which are separated by the tendinous inscription (TI) (green) viewed from posterior–medial. Top: three representative transversal US images used for segmentation. The concave TI is indicated by a green arrow, visible between the two compartments, the distal aponeurosis (apo_{dist}) – also shaped concavely – by a white arrow. Segmentation was performed on transversal images every 5 mm along the muscle belly. Bottom: the image shows the TI (green) and the distal aponeurosis (white), which are orientated in parallel to each other, but opposite in orientation of their concave shapes. Note that the image of this example for the method section was taken from a subject *in vivo*. In the voxel arrays of the cadavers a segmentation of the proximal compartment was not possible. a, anterior; BF, biceps femoris muscle; l, lateral; m, medial; p, posterior; SM, semimembranosus muscle.

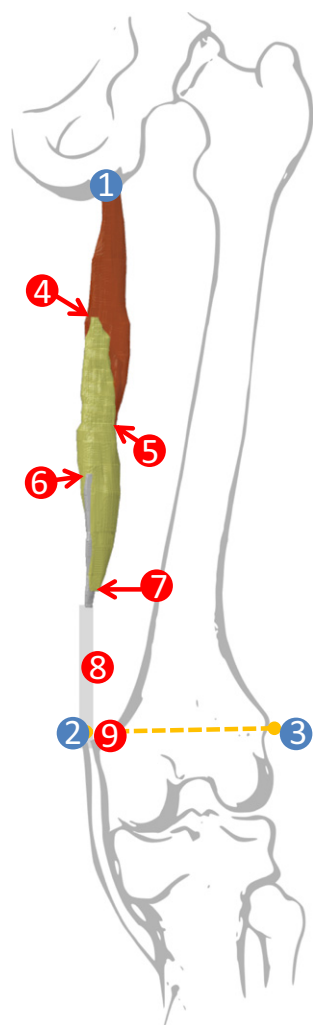


Fig. 3 Illustration of anatomical points used for analyzing three-dimensional ultrasound (3D US) imaging of semitendinosus muscle (ST). Bony landmarks (blue) and points at the ST (red): 1: ischial tuberosity; 2: medial epicondyle; 3: lateral epicondyle; 2–3: estimated knee axis; 4: proximal end of the tendinous inscription; 5: distal end of the tendinous inscription; 6: proximal end of the distal aponeurosis; 7: distal end of the most distal fascicle (i.e. distal end of muscle belly); 8: most distal point of ST tendon visible by ultrasound; 9: point where tendon passes the knee axis. Variables measured as distance between points: 1–7: muscle belly length (ℓ_m); 1–4: most proximal fascicle of proximal compartment ($\ell_{\text{fasc}_{\text{prox}_p}}$); 4–6: most proximal fascicle of distal compartment ($\ell_{\text{fasc}_{\text{dist}_p}}$); 5–7: most distal fascicle of distal compartment ($\ell_{\text{fasc}_{\text{dist}_d}}$); 6–7: distal aponeurosis ($\ell_{a_{\text{dist}}}$); and 7–9: distal tendon length till estimated knee axis ($\ell_{t_{\text{dist}_p}}$). Note that the image of this example for the method section was taken from a subject *in vivo*. In the voxel arrays of the cadavers, a segmentation of the proximal compartment was not possible.

Treatment of data and statistics

Differences between morphological characteristics assessed by 3D US and after dissection were calculated and compared using paired-samples *t*-test. To assess how comparable morphological variables assessed by 3D US are to those measured after dissection, 95% limits

of agreement (95% LoA) and ICCs were calculated. The 95% LoAs were calculated with the Bland and Altman method using the mean systematic difference between 3D US and dissection (\bar{d}) and the standard deviation of these differences (SD_{dif} ; Bland & Altman, 1986).

$$95\% \text{ LoA} = \bar{d} \pm 1.96 * SD_{\text{dif}} \quad (2)$$

The ICC for a single measurement was calculated using variance components of subject (i.e. cadaver) and method (i.e. 3D US and dissection) determined by a restricted maximum-likelihood estimation approach (Vet et al. 2011).

For variables only assessed after dissection, two-way repeated-measures ANOVAs were used to test for differences in fascicle length between compartments (proximal and distal) and between intra-compartmental locations (most distal, most proximal and intermediate). As a follow-up test for significant interaction effects, paired-sample *t*-tests with Bonferroni corrections were performed. The difference in ACSA and PCSA both assessed after dissection was determined by paired-samples *t*-tests. Paired-samples *t*-tests were also used to test whether α , β , γ , Vol , $PCSA$, $PCSA_{\text{optimum}}$, ℓ_a , ℓ_{sarc} , $\ell_{\text{fasc}_{\text{average_optimum}}}$ differed between proximal and distal compartments. The 95% confidence interval was calculated, along with Cohen's d_z determined from the *t*-value and the sample size (n) as a measure of effect size (Lakens, 2013).

$$\text{Cohen's } d_z = \frac{t}{\sqrt{n}} \quad (3)$$

Power using Cohen's d_z and $\alpha = 0.05$ were calculated *post hoc* (G*Power, Germany; Faul et al. 2007) for all variables where a proximal–distal difference was assessed.

The level of significance was set at 0.05 for all statistical tests. Values are presented as mean \pm SD.

Results

Comparison of the morphological characteristics assessed using 3D US and after dissection

All morphological variables as described in the Materials and methods section could be analyzed by 3D US in four cadavers. In two cadavers, assessment of x , y , z coordinates of the proximal end of the distal aponeurosis and/or the proximal end of the tendinous inscription was not feasible and therefore related variables could not be assessed (Table 1).

Three-dimensional US-determined ℓ_{mtc} , Vol_{dist} , ℓ_m , $\ell_{\text{fasc}_{\text{prox}_p}}$ and $\ell_{\text{fasc}_{\text{dist}_p}}$ differed < 5% from those assessed after dissection, while estimates of ACSA, $PCSA_{\text{dist}}$, $\ell_{t_{\text{dist}_p}}$, $\ell_{a_{\text{dist}}}$ and $\ell_{\text{fasc}_{\text{dist}_d}}$ were < 10% different (Table 1). For all variables assessed, 3D US-obtained measures were not significantly different from those measured in the dissected muscle, except for the most distal fascicles of the distal compartment of ST (Table 1). The lengths of fascicles at that location were systematically overestimated by 3D US by a mean value of 1.0 ± 0.9 cm (i.e. 8.9%, $P = 0.045$). ICCs were higher than 0.75 for all variables, except for fascicle length measured within the proximal compartment (ICC = 0.58; Table 1).

Morphology ST determined after dissection

Semitendinosus MTUs, that were assessed after cadaveric dissection, consisted of one-third of tendon ($\ell_{t_{\text{dist}}} = 15.0 \pm 2.0$ cm) and two-thirds of muscle belly ($\ell_m = 31.3 \pm 1.75$ cm). ACSA and PCSA did not differ ($P = 0.283$; Table 2). Repeated-measures ANOVA neither revealed significant differences in fascicle lengths between compartments (i.e. proximal and distal; $P = 0.061$) nor between locations within the compartments (i.e. most distal, intermediate and most proximal fascicles; $P = 0.377$). However, a significant interaction effect between intra-compartmental location and compartment was shown ($P = 0.001$). Follow-up analysis indicated a significant length difference between compartments only for the most distal fascicles of both compartments ($\ell_{\text{fasc}_{\text{d}}}$; Table 2). Volumes of the proximal and distal compartments were not different ($P = 0.607$). Also, for ℓ_{sarc} and $\ell_{\text{fasc}_{\text{average_optimum}}}$ no differences between both compartments were found ($P = 0.079$ and $P = 0.140$, respectively). However, PCSA and PCSA_{optimum} of the proximal compartment were significantly larger than those of the distal compartment ($P = 0.009$ and $P = 0.041$; Table 2). Measurements of angles α and β revealed small differences between proximal and distal compartments (i.e. $\alpha_{\text{prox}} < \alpha_{\text{dist}}$, $P = 0.036$ and $\beta_{\text{prox}} > \beta_{\text{dist}}$, $P = 0.032$). Angle γ did not differ between compartments ($P = 0.116$). Effect sizes (Cohen's d_z) were 0.6 or higher for all morphological variables between proximal and distal compartments, except for volume (Table 2).

Discussion

This study introduced a novel 3D US protocol to assess morphology of ST *in vivo*. Comparison of morphological

variables obtained after dissection and by 3D US revealed that the proposed 3D US protocol allows for reasonably accurate estimates of key morphological characteristics of ST muscle. ICCs for ℓ_{mtu} , ℓ_m and ℓ_{fasc} were at least similar or higher than those reported previously for two-dimensional US measurements of ST (Kellis et al. 2009), based on the same number of cadaveric muscles.

The current estimates of ST morphological variables obtained using 3D US imaging did not differ from those measured after cadaveric dissection, except for $\ell_{\text{fasc}_{\text{dist}_{\text{d}}}}$, which was systematically overestimated. $\ell_{\text{fasc}_{\text{dist}_{\text{d}}}}$ was defined as the distance between the distal end of the most distal fascicle and distal end of the tendinous inscription. The distal end of the most distal fascicle was also used for calculation of ℓ_m and $\ell_{t_{\text{dist}_{\text{p}}}}$, for which no significant difference between both types of measurements was found. Therefore, it was concluded that the overestimation of $\ell_{\text{fasc}_{\text{dist}_{\text{d}}}}$ was caused by erroneous localization of the distal end of the tendinous inscription proximal to its actual location. This may occur because the tendinous inscription is distally very closely aligned with the epimysium. Within the voxel array the tendinous inscription can only be visually distinguished from the epimysium when the tendinous inscription is clearly diverging from the epimysium.

For the proximal fascicle length ($\ell_{\text{fasc}_{\text{prox}_{\text{p}}}}$), the ICC was relatively low (0.58). Estimation of $\ell_{\text{fasc}_{\text{prox}_{\text{p}}}}$ was most likely affected by a lower quality of images from the most proximal region of ST compared with those from the middle and distal regions. This made it more difficult to assess x , y , z coordinates of the points (i.e. proximal end of the tendinous inscription and ischial tuberosity) within the voxel array. Also due to the limited image quality, it was not possible to determine the volume of the proximal

Table 1 Morphological characteristics of ST of six cadavers obtained by 3D US and after dissection.

Morphological characteristics	<i>n</i>	3D US	Dissection	Difference between methods	ICC	95% upper LoA	95% lower LoA
ℓ_{mtu}	6	38.4 ± 3.3 cm	37.7 ± 2.5 cm	-0.7 cm (1.9%)	0.87	2.1 cm	-3.5 cm
Vol_{dist}	5	38.4 ± 7.4 cm ³	38.4 ± 7.5 cm ³	0.0 cm ³ (0.0%)	0.96	4.6 cm ³	-4.6 cm ³
ℓ_m	6	31.6 ± 2.6 cm	31.3 ± 1.7 cm	-0.3 cm (1.0%)	0.83	2.4 cm	-3.0 cm
$\ell_{t_{\text{dist}_{\text{p}}}}$	6	6.8 ± 1.0 cm	6.4 ± 1.2 cm	-0.4 cm (6.6%)	0.80	0.8 cm	-1.6 cm
$\ell_{a_{\text{dist}}}$	5	14.0 ± 2.7 cm	13.2 ± 3.7 cm	-0.8 cm (6.2%)	0.91	1.6 cm	-3.2 cm
$\ell_{\text{fasc}_{\text{dist}_{\text{d}}}}$	6	12.3 ± 1.7 cm	11.3 ± 1.7 cm	-1.0 cm* (8.9%)	0.75	0.8 cm	-2.8 cm
$\ell_{\text{fasc}_{\text{dist}_{\text{p}}}}$	4	8.3 ± 1.3 cm	8.3 ± 1.2 cm	0.0 cm (0.4%)	0.99	0.4 cm	-0.3 cm
$\ell_{\text{fasc}_{\text{prox}_{\text{p}}}}$	5	9.2 ± 2.5 cm	8.9 ± 1.0 cm	-0.3 cm (3.3%)	0.58	3.4 cm	-4.0 cm
ACSA	5	4.6 ± 1.2 cm ²	4.2 ± 1.0 cm ²	-0.4 cm ² (9.5%)	0.91	0.1 cm ²	-0.9 cm ²
PCSA _{dist}	4	4.0 ± 1.1 cm ²	4.2 ± 1.3 cm ²	+0.2 cm ² (6.0%)	0.90	1.3 cm ²	-0.8 cm ²

*Significantly different between dissection and 3D US ($P < 0.05$); values in parentheses are percentages of the dissection mean group values.

3D, three-dimensional; ACSA, anatomical cross-sectional area; ICC, intra-class correlation coefficients; LoA, limit of agreement; ℓ_{mtu} , length of muscle-tendon complex till estimated knee axis as the sum of ℓ_m and $\ell_{t_{\text{dist}_{\text{p}}}}$; Vol_{dist} , muscle volume of the distal compartment; ℓ_m , length muscle belly, ischial tuberosity to distal muscle tendinous junction; $\ell_{t_{\text{dist}_{\text{p}}}}$, length of distal tendon proximal of the estimated knee axis; $\ell_{\text{fasc}_{\text{dist}_{\text{d}}}}$, most distal fascicle of distal compartment; $\ell_{\text{fasc}_{\text{dist}_{\text{p}}}}$, most proximal fascicles of distal compartment; $\ell_{\text{fasc}_{\text{prox}_{\text{p}}}}$, most proximal fascicles of proximal compartment; PCSA_{dist}, physiological cross-sectional area of distal compartment; PCSA_{dist} = $Vol_{\text{dist}} / ((\ell_{\text{fasc}_{\text{dist}_{\text{d}}} + \ell_{\text{fasc}_{\text{dist}_{\text{p}}}}) / 2)$; US, ultrasound.

Table 2 Morphological characteristics of ST from cadaveric dissection from six cadavers for distal and proximal compartment [mean \pm standard deviation, 95% confidence interval, and effect size (Cohen's d_2)].

	Proximal compartment	Distal compartment	Whole muscle	Difference between compartments P-value	95% CI	Effect size	Power
Vol (cm ³)	39.0 \pm 8.3	38.0 \pm 6.8	77.0 \pm 15.1	0.607	-3.7 to 5.7	0.2	0.07
la (cm)	11.3 \pm 1.7	13.0 \pm 3.3	n/a	0.077	-3.7 to 0.3	0.9	0.44
lfasc _p (cm)	8.9 \pm 0.9	8.0 \pm 1.2	16.9 \pm 1.1	0.684	-0.9 to 2.8	0.6	0.20
lfasc _m (cm)	8.1 \pm 1.2	9.7 \pm 1.7	17.8 \pm 2.1	0.291	-3.8 to 0.4	0.8	0.38
lfasc _d (cm)	7.0 \pm 1.5	11.3 \pm 1.7	18.3 \pm 1.9	0.027	-7.0 to -1.7	1.7	0.91
lfasc _{average} (cm)	8.0 \pm 0.8	9.7 \pm 1.2	17.7 \pm 1.1	0.061	-3.4 to 0.1	1.0	0.49
lsarc (μ m)	2.82 \pm 0.10	3.00 \pm 0.19	2.91 \pm 0.11	0.079	-0.40 to 0.03	0.9	0.43
lfasc _{average_optimum} (cm)	7.7 \pm 0.7	8.7 \pm 1.0	16.4 \pm 0.8	0.140	-2.6 to 0.5	0.7	0.30
α ($^\circ$)	1.7 \pm 3.2	10.2 \pm 5.2	n/a	0.032	1.7-24.9	1.2	0.65
β ($^\circ$)	18.0 \pm 10.4	4.8 \pm 3.2	n/a	0.036	-16.3 to -0.8	1.2	0.63
γ ($^\circ$)	19.7 \pm 8.4	15.0 \pm 5.0	n/a	0.116	-1.7 to 11.2	0.8	0.34
ACSA (cm ²)	-	-	4.2 \pm 1.0	-	-	-	-
PCSA (cm ²)	4.9 \pm 0.9	4.0 \pm 1.1	4.4 \pm 1.0	0.009	0.3-1.3	1.7	0.91
PCSA _{optimum} (cm ²)	5.1 \pm 0.9	4.4 \pm 1.0	4.7 \pm 0.9	0.041	0.4-1.3	1.1	0.60

ACSA, anatomical cross-sectional area; CI, confidence interval; Vol, muscle volume; la, length aponeurosis; lfasc_p, length most proximal fascicle; lfasc_m, length intermediate fascicle; lfasc_d, length most distal fascicle; lfasc_{average} = average lfasc_p, lfasc_m and lfasc_d; lsarc, mean length of sarcomeres; lfasc_{average_optimum}, calculated at optimum lsarc (i.e. 2.7 μ m); α , angle of the muscle line of pull with fascicles; β , angle of the muscle line of pull with the aponeurosis; $\gamma = \alpha + \beta$; PCSA, physiological cross-sectional area; PCSA = Vol/lfasc_{average}; PCSA_{optimum} = Vol/lfasc_{average_optimum}.

compartment using 3D US. The lower image quality proximally compared with distally was probably caused by a thicker layer of subcutaneous tissue and by the m. gluteus. US image quality of muscle tissue *in vivo* is known to be higher than in formalin-preserved cadavers (Tsui et al. 2007). In addition, estimates of positions of bony landmarks (especially the location of the ischial tuberosity) *in vivo* are expected to be more accurate than in cadavers, because in live subjects these landmarks can be identified easier by palpation (i.e. due to more compliant tissues and flexibility of joints). Regarding the estimation of the proximal ST volume, it was expected that this can also be estimated accurately if the borders of the muscle are sufficiently visible and, thus, can be segmented within the voxel array. This expectation is confirmed by results for the distal compartment and by other studies that have shown that if a muscle can be accurately segmented valid measurements of muscle volume of different muscles are possible (Weller et al. 2007; Barber et al. 2009; MacGillivray et al. 2009). Segmentation of the proximal volume of ST is expected to be limited also *in vivo* in subjects with a very thick layer of subcutaneous tissue and/or a large m. gluteus.

Anatomical cross-sectional area was measured perpendicular to the line of pull. Because the angle of the fascicles with the line of pull was shown to be very low, ACSA of ST did not differ from PCSA. Regarding the measurements of PCSAs in the cadavers using 3D US, it was only possible to assess PCSA of the distal compartment. However, if the

proximal volume of the ST can be assessed, the described 3D US protocol will allow the calculation of PCSA of the whole ST. Within the proximal compartment, only the length of the most proximal fascicles (i.e. lfasc_{prox_p}) can be assessed by 3D US. Because of the non-uniformity of fascicle length within compartments, lfasc_{prox_p} cannot be used to assess PCSA_{prox}. The observation that fascicle lengths within a compartment are not uniform is in line with local differences in sarcomere numbers in other human leg muscles (Huijing, 1985). When assessing fascicle lengths and PCSAs of each ST compartment, this non-uniformity in length has to be considered.

No differences in fascicle lengths between distal and proximal compartments were found, except for the most distal fascicles at both compartments (lfasc_d). Similar fascicle lengths within the two compartments (Wickiewicz et al. 1983; Woodley & Mercer, 2005; Kellis et al. 2012), as well as shorter fascicle lengths in the proximal compared with the distal compartment (Markee et al. 1955), have been reported. However, comparison of the results between the present data and those of previous studies regarding differences in fascicle lengths within and between compartments is hampered by a lack of standardization of the location of the measured fascicles or differences in the dissection plane. The absence of significant proximal-distal differences in the current and above-described studies may have been the result of low statistical power. Based on the observation that no differences

were found between proximal and distal volumes, while PCSAs of both compartments were significantly different, one would expect also a difference in fascicle length ($\ell_{\text{fasc}_{\text{average_optimum}}}$) between the compartments. Power calculations using the effect size (Table 2), $\alpha = 0.05$ and $\beta = 0.80$ (G*Power, Germany; Faul et al. 2007) revealed that at least 19 subjects would have been required to confirm proximal–distal differences for ℓ_a , $\ell_{\text{fasc}_{\text{m}}}$, $\ell_{\text{fasc}_{\text{average}}}$ and $\ell_{\text{fasc}_{\text{average_optimum}}}$ (12, 15, 10 and 19 subjects, respectively).

Muscle belly length, tendon length, fascicle length as well as sarcomere length of the current specimen were comparable to those reported previously (Markee et al. 1955; Wickiewicz et al. 1983; Cutts, 1988; Friederich & Brand, 1990; Woodley & Mercer, 2005; Kellis et al. 2009, 2010; Ward et al. 2009; van der Made et al. 2013). Note that morphological variables of ST in the current study and in most of the previous studies were determined in cadavers that were of a high age. This should be taken into account when absolute values are compared with subjects of younger age, but it does not bias the comparison between 3D US and dissection. Particularly, PCSA and muscle volumes of ST can be expected to be larger for younger people (Nishino et al. 2006). Assuming that aging effects are comparable at different locations and compartments of ST, the presented relative differences and similarities between and within compartments of ST are representative in all age groups.

Possible applications

The proposed 3D US protocol yields promising results to measure important morphological variables of ST *in vivo*. Multiple freehand 3D US measurements can be easily performed, for example at different knee and hip joint angles (Haberfehlner et al. 2015). Measurements of lengths of muscle and tendon may provide insight into differences in their stiffness. This information is relevant to understand the effects of alterations of ST muscle on movement limitations around the knee in patients (e.g. cerebral palsy or patients after an anterior cruciate ligament reconstruction using the ST tendon).

Acknowledgements

The authors wish to thank Henk Schutte, Guus Baan, Wendy Noort and Guido Weide for their assistance with this study. The students who assisted in the dissection work during the course anatomy at the Department of Human Movement Sciences (Vrije Universiteit, Amsterdam) are acknowledged. The authors are very grateful to Adam Shortland and Nicola Fry who shared their algorithms of 3D US, which were the basis for the Matlab programs used in this study.

This research is financially supported by the Phelps Stichting voor Spastici, Bussum, The Netherlands. Huub Maas was supported by the Division for Earth and Life Sciences of the Netherlands Organization for Scientific Research (864-10-011).

References

- Alexander RM, Vernon A (1975) The dimensions of knee and ankle muscles and the forces they exert. *J Hum Mov Stud* **1**, 115–123.
- Baldwin SL, Marutyan KR, Yang M, et al. (2006) Measurements of the anisotropy of ultrasonic attenuation in freshly excised myocardium. *J Acoust Soc Am* **119**, 3130–3139.
- Bamber JC, Hill CR, King JA, et al. (1979) Ultrasonic propagation through fixed and unfixed tissues. *Ultrasound Med Biol* **5**, 159–165.
- Barber L, Barrett R, Lichtwark G (2009) Validation of a freehand 3D ultrasound system for morphological measures of the medial gastrocnemius muscle. *J Biomech* **42**, 1313–1319.
- Bénard MR, Harlaar J, Becher JG, et al. (2011) Effects of growth on geometry of gastrocnemius muscle in children: a three-dimensional ultrasound analysis. *J Anat* **219**, 388–402.
- Bland JM, Altman DG (1986) Statistical methods for assessing agreement between two methods of clinical measurement. *Lancet* **1**, 307–310.
- Brand RA, Pedersen DR, Friederich JA (1986) The sensitivity of muscle force predictions to changes in physiologic cross-sectional area. *J Biomech* **19**, 589–596.
- Cutts A (1988) The range of sarcomere lengths in the muscles of the human lower limb. *J Anat* **160**, 79–88.
- Faul F, Erdfelder E, Lang AG, et al. (2007) G*Power 3: a flexible statistical power analysis program for the social, behavioral, and biomedical sciences. *Behav Res Methods* **39**, 175–191.
- Friederich JA, Brand RA (1990) Muscle fiber architecture in the human lower limb. *J Biomech* **23**, 91–95.
- Fry NR, Gough M, Shortland AP (2004) Three-dimensional realisation of muscle morphology and architecture using ultrasound. *Gait Posture* **20**, 177–182.
- Gage JR, Schwartz MH, Koop SE, et al. (2009) *The identification and treatment of gait problems in cerebral palsy*. Mac Keith: Cambridge University Press, London.
- Gans C, Bock WJ (1965) The functional significance of muscle architecture – a theoretical analysis. *Ergeb Anat Entwicklungsgesch* **38**, 115–142.
- Gans C, Gaunt AS (1991) Muscle architecture in relation to function. *J Biomech* **24**(Suppl 1), 53–65.
- Haberfehlner H, Maas H, Harlaar J, et al. (2015) Assessment of net knee moment-angle characteristics by instrumented hand-held dynamometry in children with spastic cerebral palsy and typically developing children. *J Neuroeng Rehabil* **12**, 67.
- Huijing PA (1985) Architecture of the human gastrocnemius muscle and some functional consequences. *Acta Anat (Basel)* **123**, 101–107.
- Huijing PA (1996) Important experimental factors for skeletal muscle modelling: non-linear changes of muscle length force characteristics as a function of degree of activity. *Eur J Morphol* **34**, 47–54.
- Keenan MA, Ure K, Smith CW, et al. (1988) Hamstring release for knee flexion contracture in spastic adults. *Clin Orthop Relat Res* **236**, 221–226.
- Kellis E, Galanis N, Natsis K, et al. (2009) Validity of architectural properties of the hamstring muscles: correlation of ultrasound findings with cadaveric dissection. *J Biomech* **42**, 2549–2554.
- Kellis E, Galanis N, Natsis K, et al. (2010) Muscle architecture variations along the human semitendinosus and biceps femoris (long head) length. *J Electromyogr Kinesiol* **20**, 1237–1243.

- Kellis E, Galanis N, Natsis K, et al. (2012) *In vivo* and *in vitro* examination of the tendinous inscription of the human semitendinosus muscle. *Cells Tissues Organs* **195**, 365–376.
- Lakens D (2013) Calculating and reporting effect sizes to facilitate cumulative science: a practical primer for t-tests and ANOVAs. *Front Psychol* **4**, 863.
- Lee TC, O'Driscoll KJ, McGettigan P, et al. (1988) The site of the tendinous interruption in semitendinosus in man. *J Anat* **157**, 229–231.
- Lieber RL, Loren GJ, Friden J (1994) *In vivo* measurement of human wrist extensor muscle sarcomere length changes. *J Neurophysiol* **71**, 874–881.
- MacGillivray TJ, Ross E, Simpson HA, et al. (2009) 3D freehand ultrasound for *in vivo* determination of human skeletal muscle volume. *Ultrasound Med Biol* **35**, 928–935.
- van der Made AD, Wieldraaijer T, Kerkhoffs GM, et al. (2015) The hamstring muscle complex. *Knee Surg Sports Traumatol Arthrosc* **23**, 2115–2122.
- Markee JE, Logue JT Jr, Williams M, et al. (1955) Two-joint muscles of the thigh. *J Bone Joint Surg Am*, **37-A**, 125–142.
- Martin JN, Vialle R, Denormandie P, et al. (2006) Treatment of knee flexion contracture due to central nervous system disorders in adults. *J Bone Joint Surg Am* **88**, 840–845.
- Nishino A, Sanada A, Kanehisa H, et al. (2006) Knee-flexion torque and morphology of the semitendinosus after ACL reconstruction. *Med Sci Sports Exerc* **38**, 1895–1900.
- Pettersen EF, Goddard TD, Huang CC, et al. (2004) UCSF Chimera – a visualization system for exploratory research and analysis. *J Comput Chem* **25**, 1605–1612.
- Prager RW, Rohling RN, Gee AH, et al. (1998) Rapid calibration for 3-D freehand ultrasound. *Ultrasound Med Biol* **24**, 855–869.
- Rassier DE, MacIntosh BR, Herzog W (1999) Length dependence of active force production in skeletal muscle. *J Appl Physiol* (1985) **86**, 1445–1457.
- Schindelin J, Arganda-Carreras I, Frise E, et al. (2012) Fiji: an open-source platform for biological-image analysis. *Nat Methods* **9**, 676–682.
- Schneider CA, Rasband WS, Eliceiri KW (2012) NIH Image to ImageJ: 25 years of image analysis. *Nat Methods* **9**, 671–675.
- Silder A, Heiderscheid BC, Thelen DG, et al. (2008) MR observations of long-term musculotendon remodeling following a hamstring strain injury. *Skeletal Radiol* **37**, 1101–1109.
- Straube WL, Arthur RM (1994) Theoretical estimation of the temperature dependence of backscattered ultrasonic power for noninvasive thermometry. *Ultrasound Med Biol* **20**, 915–922.
- Tijs C, van Dieen JH, Maas H (2015) Effects of epimuscular myofascial force transmission on sarcomere length of passive muscles in the rat hindlimb. *Physiol Rep* **3**, e12608.
- Tsui BC, Dillane D, Pillay J, et al. (2007) Cadaveric ultrasound imaging for training in ultrasound-guided peripheral nerve blocks: lower extremity. *Can J Anaesth* **54**, 475–480.
- Vet HCW, Terwee CB, Mokkink LB, et al. (2011) *Measurement in Medicine*. New York: Cambridge University Press.
- Walker SM, Schrodt GR (1974) I segment lengths and thin filament periods in skeletal muscle fibers of the Rhesus monkey and the human. *Anat Rec* **178**, 63–81.
- Ward SR, Eng CM, Smallwood LH, et al. (2009) Are current measurements of lower extremity muscle architecture accurate? *Clin Orthop Relat Res* **467**, 1074–1082.
- Weide G, Huijijng PA, Maas JC, et al. (2015) Medial gastrocnemius muscle growth during adolescence is mediated by increased fascicle diameter rather than by longitudinal fascicle growth. *J Anat* **226**, 530–541.
- Weller R, Pfau T, Ferrari M, et al. (2007) The determination of muscle volume with a freehand 3D ultrasonography system. *Ultrasound Med Biol* **33**, 402–407.
- Wickiewicz TL, Roy RR, Powell PL, et al. (1983) Muscle architecture of the human lower limb. *Clin Orthop Relat Res* **179**, 275–283.
- Winters TM, Takahashi M, Lieber RL, et al. (2011) Whole muscle length-tension relationships are accurately modeled as scaled sarcomeres in rabbit hindlimb muscles. *J Biomech* **44**, 109–115.
- Woittiez RD, Huijijng PA, Rozendal RH (1983) Influence of muscle architecture on the length-force diagram of mammalian muscle. *Pflugers Arch* **399**, 275–279.
- Woodley SJ, Mercer SR (2005) Hamstring muscles: architecture and innervation. *Cells Tissues Organs* **179**, 125–141.